Research in Astron. Astrophys. **2010** Vol. **10** No. **10**, 1013–1022
http://www.raa-journal.org *http://www.iop.org/journals/raa*

***R**esearch in*
***A**stronomy and*
***A**strophysics*

Central gas entropy excess as direct evidence for AGN feedback in galaxy groups and clusters*

Yu Wang[1], Hai-Guang Xu[1], Jun-Hua Gu[1], Li-Yi Gu[1], Jing-Ying Wang[1] and Zhong-Li Zhang[2]

[1] Department of Physics, Shanghai Jiao Tong University, Shanghai 200240, China; *wangyu@shao.ac.cn*; *hgxu@sjtu.edu.cn*
[2] Max-Planck-Institute for Astrophysics, Karl-Schwarzschild-Str. 1, Postfach 1317 D-85741, Garching, Germany

Received 2010 February 9; accepted 2010 June 3

Abstract By analyzing *Chandra* X-ray data of a sample of 21 galaxy groups and 19 galaxy clusters, we find that in 31 sample systems there exists a significant central ($R \lesssim 10\,h_{71}^{-1}$ kpc) gas entropy excess (ΔK_0), which corresponds to $\simeq 0.1 - 0.5$ keV per gas particle, beyond the power-law model that best fits the radial entropy profile of the outer regions. We also find a distinct correlation between the central entropy excess ΔK_0 and K-band luminosity L_K of the central dominating galaxies (CDGs), which is scaled as $\Delta K_0 \propto L_K^{1.6\pm0.4}$, where L_K is tightly associated with the mass of the supermassive black hole hosted in the CDG. In fact, if an effective mass-to-energy conversion-efficiency of 0.02 is assumed for the accretion process, the cumulative AGN feedback $E_{\rm feedback}^{\rm AGN} \simeq \eta M_{\rm BH} c^2$ yields an extra heating of $\simeq 0.5 - 17.0$ keV per particle, which is sufficient to explain the central entropy excess. In most cases, the AGN contribution can compensate the radiative loss of the X-ray gas within the cooling radius ($\simeq 0.002 - 2.2$ keV per particle), and apparently exceeds the energy required to cause the scaling relations to deviate from the self-similar predictions ($\simeq 0.2 - 1.0$ keV per particle). In contrast to the AGN feedback, the extra heating provided by supernova explosions accounts for $\simeq 0.01 - 0.08$ keV per particle in groups and is almost negligible in clusters. Therefore, the observed correlation between ΔK_0 and L_K can be considered as direct evidence for AGN feedback in galaxy groups and clusters.

Key words: galaxies: active — galaxies: clusters: general — X-rays: galaxies: clusters — (galaxies:) intergalactic medium

1 INTRODUCTION

Over the past few decades, many observational and theoretical efforts have been devoted to the studies of galaxy groups and clusters. As of today, however, some fundamental astrophysical processes that determine the basic properties of these celestial systems are still poorly understood. For example, the scaling relations between X-ray luminosity ($L_{\rm X}$), gas temperature ($T_{\rm X}$), gas entropy (K), and

* Supported by the National Natural Science Foundation of China.

total gravitating mass ($M_{\rm total}$), which are predicted by the self-similar gravitational collapse scenario (e.g., Kaiser 1986; Navarro, Frenk & White 1995), are challenged by observed deviations in such a distinct way that non-gravitational heating sources are invoked to dominate the gas heating process in the central $\simeq$100 kpc (e.g., Ponman et al. 2003; Donahue et al. 2006; Sun et al. 2009). Currently, most of the efforts have been focused on the AGN heating of the inter-galactic medium (IGM) (see McNamara & Nulsen 2007 for a review), since it is estimated that powerful AGN outbursts may repeat per $10^6 - 10^8$ yr and release $10^{58} - 10^{62}$ erg per outburst into the environment, and this amount of energy is sufficient to balance gas cooling and heating on the scales of groups and clusters (e.g., Rafferty et al. 2006, 2008; Birzan et al. 2009).

However, problems also exist in the AGN feedback scenario. For example, the absence of X-ray cavities, a natural product of the AGN activity, has been reported in about 40% of cool core systems (e.g., Cavagnolo et al. 2008; Birzan et al. 2009), and only about 10% of quasars are found to host powerful radio jets (e.g., White et al. 2007), which indicates that cavity- and jet-related feedbacks might not be generic. In NGC 4051, the observed mass and energy outflow rates due to the AGN activity is $4-5$ orders of magnitude below those required for efficient feedback (Mathur et al. 2009). Also, Jetha et al. (2007) reported that no significant difference of gas entropy profiles between radio-loud and radio-quiet galaxy groups is found (see also Sun et al. 2009).

If AGN feedback does dominate the gas heating history in central regions of galaxy groups and clusters, it should be proportional to the central gas entropy excess ΔK, i.e., $E^{\rm AGN}_{\rm feedback} \propto \Delta K$ (Voit & Donahue 2005), where ΔK is measured beyond a power-law model that best describes the gas entropy distribution in the intermediate and outer regions. On the other hand, by studying AGN cavities embedded in the X-ray halos of galaxy groups and clusters, Allen et al. (2006) found a close relation between the AGN feedback energy $E^{\rm AGN}_{\rm feedback}$ and the Bondi accretion power $P_{\rm Bondi} = \eta \dot{M} c^2 \propto M^2_{\rm BH}$ (η is the mass-to-energy conversion efficiency, $\dot{M}$ is the accretion rate, and $M_{\rm BH}$ is the black hole mass; Bondi 1952), which indicates that the AGN feedback should scale with the SMBH mass in the form of $E^{\rm AGN}_{\rm feedback} \propto M^2_{\rm BH}$. In addition, we know that $M_{\rm BH}$ is related to the galaxy's bulge luminosity $L_{\rm bulge}$ and thus the galaxy's K-band luminosity L_K via $M_{\rm BH} \propto L_{\rm bulge} \propto L_K$ (Marconi & Hunt 2003; Batcheldor et al. 2007). Given the above relations, we expect a tight correlation between the central gas entropy excess and the galaxy's K-band luminosity, i.e., $\Delta K \propto L^2_K$, which has never been reported in literature.

In order to examine whether this correlation holds or not, we analyze the *Chandra* archive data of a sample of 21 galaxy groups and 19 galaxy clusters to measure the central gas entropy excesses, and then compare them with the K-band luminosities of central dominating galaxies (CDGs). In Section 2 we describe our sample, the *Chandra* observations, and data reduction. In Section 3 we measure gas density and temperature, and study the central gas entropy excess against L_K. In Sections 4 and 5 we discuss and summarize our results, respectively. Throughout the paper, we adopt the cosmological parameters $H_0 = 71\,{\rm km\,s^{-1}\,Mpc^{-1}}$, $\Omega_b = 0.044$, $\Omega_M = 0.27$, and $\Omega_\Lambda = 0.73$. Unless stated otherwise, the quoted errors stand for the 90% confidence limits.

2 SAMPLE, OBSERVATION, AND DATA REDUCTION

2.1 Sample Selection

In order to achieve our scientific goal, we need to select bright, nearby galaxy groups and clusters whose central galaxy can be well resolved with the *Chandra* Advanced CCD Imaging Spectrometer (ACIS). To investigate the interaction between the central AGN and the IGM, the selected systems are limited to having only one bright central-dominating galaxy and show no significant merger signatures. Our sample consists of the 20 brightest nearby ($z < 0.1$) galaxy groups and clusters selected from the flux-limited *ASCA* sample of Ikebe et al. (2002), and 18 galaxy groups from two *ROSAT* group samples constructed by Mulchaey et al. (2003) and Osmond & Ponman (2004), respectively. In addition, we add the group NGC 3402 ($z = 0.0153$), which satisfies the sample selection criteria,

and the giant AGN cavity cluster MS 0735.6+7421 ($z = 0.216$) for comparison. All the selected systems lie outside the Galactic latitudes of ±15°, and are located outside the fields of the Magellanic Clouds. Some basic properties of the sample members are summarized in Table 1.

Table 1 The Sample

Group/cluster	Redshift	CDG	$\log(L_B/L_{B,\odot})$ [a]	$\log(L_K/L_{K,\odot})$ [b]	Chandra observation		
					ObsID	Date	Raw (net) exposure (ks)
NGC 0383	0.0173	NGC 0383	10.86	11.71±0.01	2147	2000–11–06	47.2 (44.4)
NGC 0507	0.0170	NGC 0507	11.02	11.76±0.01	2882	2002–01–08	43.7 (43.4)
NGC 0533	0.0181	NGC 0533	11.07	11.75±0.01	2880	2002–07–28	37.6 (37.4)
NGC 0720	0.0059	NGC 0720	10.49	11.25±0.01	7372	2006–08–06	49.4 (48.8)
NGC 0741	0.0185	NGC 0741	11.19	11.84±0.01	2223	2001–01–28	30.4 (29.6)
NGC 1407	0.0057	NGC 1407	10.77	11.46±0.01	791	2000–08–16	48.6 (48.6)
NGC 2563	0.0159	NGC 2563	10.59	11.42±0.01	7925	2007–09–18	48.8 (47.9)
NGC 3402	0.0153	NGC 3402	10.76	11.42±0.01	3243	2002–11–05	29.5 (29.3)
NGC 4125	0.0050	NGC 4125	10.70	11.28±0.01	2071	2001–09–09	64.2 (63.6)
NGC 4261	0.0068	NGC 4261	10.72	11.38±0.01	9569	2008–02–12	101.0 (99.3)
NGC 4325	0.0254	NGC 4325	10.66	11.30±0.02	3232	2003–02–04	30.1 (29.9)
NGC 5044	0.0082	NGC 5044	10.85	11.37±0.01	9399	2008–03–07	82.7 (82.7)
NGC 5129	0.0233	NGC 5129	11.07	11.65±0.01	6944	2006–04–13	21.0 (21.0)
					7325	2006–04–14	26.7 (25.8)
NGC 5846	0.0063	NGC 5846	10.70	11.45±0.01	7923	2007–06–12	90.4 (89.8)
NGC 6269	0.0353	NGC 6269	11.38	11.95±0.01	4972	2003–12–29	41.4 (39.6)
NGC 7619	0.0116	NGC 7619	10.98	11.54±0.01	3955	2003–09–24	37.5 (28.8)
HCG 42	0.0128	NGC 3091	10.88	11.60±0.01	3215	2002–03–26	31.7 (31.7)
MKW 3S	0.0450	NGC 5920	11.02	11.57±0.02	900	2000–04–03	59.1 (57.2)
MKW 4	0.0201	NGC 4073	11.14	11.83±0.01	3234	2002–11–24	30.0 (29.9)
MKW 4S	0.0286	NGC 4104	11.20	11.97±0.01	6939	2006–02–16	37.1 (35.8)
UGC 12064	0.0166	UGC 12064	10.48	11.12±0.01	4057	2003–09–18	29.2 (21.4)
2A0335+096	0.0349	PGC 013424	11.21	11.83±0.02	919	2000–09–06	21.4 (19.7)
Abell 0085	0.0556	PGC 002501	11.23	12.05±0.02	904	2000–08–19	40.5 (38.4)
Abell 0262	0.0161	NGC 0708	10.60	11.61±0.01	7921	2006–11–20	111.9 (110.7)
Abell 0478	0.0900	PGC 014685	11.32	12.04±0.03	1669	2001–01–27	42.4 (42.4)
					6102	2004-09-13	10.4 (9.9)
Abell 0496	0.0328	PGC 015524	11.18	11.87±0.02	4976	2004–07–22	75.1 (63.6)
Abell 0780	0.0538	3C 218	11.38	11.70±0.03	4970	2004–10–22	100.7 (98.8)
Abell 1651	0.0850	PGC 088678	11.00	12.42±0.04	4185	2003–03–02	9.7 (9.6)
Abell 1795	0.0616	PGC 049005	11.01	11.93±0.03	493	2000–03–21	21.3 (19.6)
Abell 2029	0.0767	IC 1101	11.33	12.31±0.02	4977	2004–01–08	77.9 (77.7)
Abell 2052	0.0348	3C 317	10.87	11.87±0.02	5807	2006–03–24	127.0 (126.9)
Abell 2063	0.0354	PGC 054913	10.79	11.67±0.02	6263	2005–03–29	16.8 (16.8)
Abell 2199	0.0302	NGC 6166	11.38	11.90±0.01	497	2000–05–13	21.5 (19.2)
Abell 2589	0.0416	NGC 7647	10.95	11.85±0.02	7190	2006–06–11	53.8 (53.4)
Abell 3112	0.0750	PGC 012264	11.35	12.15±0.03	2516	2001–09–15	17.5 (16.5)
Abell 3558	0.0480	PGC 047202	11.39	12.17±0.02	1646	2001–04–14	14.4 (14.2)
Abell 3571	0.0397	PGC 048896	11.55	12.08±0.01	4203	2003–07–31	34.0 (31.6)
Abell 4038	0.0283	IC 5358	10.95	11.68±0.02	4992	2004–06–28	33.5 (33.5)
Abell 4059	0.0460	PGC 073000	11.32	12.00±0.02	5785	2005–01–26	92.4 (92.1)
MS 0735.6+7421	0.2160	4C +74.13	11.11	11.85±0.07	4197	2003–11–30	45.9 (44.9)

[a] *B*-band luminosities of the CDGs shown as $\log(L_B/L_{B,\odot})$, which are calculated using the data drawn from *http://leda.univ-lyon1.fr* (Paturel et al. 2003).

[b] 2MASS *K*-band luminosities of the CDGs shown as $\log(L_K/L_{K,\odot})$, which are calculated using the data drawn from *http://www.ipac.caltech.edu/2mass.*

2.2 Observation and Data Reduction

All the *Chandra* observations (Table 1) were performed with the ACIS instrument operating at a focal plane temperature of −120°C, and all the selected galaxy groups and clusters were positioned close to the nominal aim point on CCD 7 (ACIS-S) or on CCD 3 (ACIS-I). We employed the *Chandra* data analysis package CIAO v4.1 and the calibration CALDB v4.1.2 to process the datasets in the standard way, by starting with the Level-1 event files. We kept events with *ASCA* grades 0, 2, 3, 4, and 6, removed all the bad pixels and bad columns, and performed corrections for both the charge transfer inefficiency (CTI) and time dependent gain. We selected regions located as far away from the galaxy groups and clusters as possible to extract the 0.3 – 10.0 keV and 2.5 – 7.0 keV lightcurves for front-illuminated CCDs (CCD 0 – 3) and back-illuminated CCDs (CCD 5 & 7), respectively, and then checked if there were occasional background flares, the intervals contaminated by which were excluded from our study. In the spectral analysis that follows, we mask all the X-ray point sources detected in 0.3 – 8.0 keV with the CIAO tool *celldetect*, and apply the spectra extracted from *Chandra* blank-sky fields as the background. When source free regions were available in the observations, we also attempted to use the spectra extracted from these regions as the background; we found that the results obtained with both background sets are consistent with each other within the 90% error limits.

3 SPECTRAL ANALYSIS AND RESULTS

3.1 Model Fittings

In order to measure the spatial distribution of specific gas entropy, which is defined as $K = kTn_{\rm e}^{-2/3}$, where T and $n_{\rm e}$ are gas temperature and electron density, respectively, we divide each galaxy group or cluster into concentric annuli, and study the spectra extracted therein with XSPEC v12.4.0 by applying a model that consists of an APEC component to represent the gas emission and a power-law component to represent the emission from unresolved point sources, both subject to a common absorption due to the neutral hydrogen. We set the metal abundance free to vary and fix the absorption at the Galactic value (Dickey & Lockman 1990), except that in 2A 0335+096 and Abell 478 the absorption is left free, because in these two galaxy clusters significant absorption excesses were reported in previous works (Mazzotta et al. 2003; Sanderson et al. 2005). We adopt the *projct* model embedded in the XSPEC package to correct the projection effect. By applying the F-test, we find that in the central annuli of the NGC 383, NGC 741, NGC 1407, NGC 4261, and NGC 5129 groups, the power-law component is required at the 90% confidence level, while in outer regions of these groups, the power-law component is negligible. In other sample systems, the contribution of the power-law component is negligibly small.

Using the best-fit deprojected spectral parameters, we calculate the 3-dimensional azimuthally-averaged radial entropy distribution $K(R)$ for all the sample systems and plot them in Figure 1. Following Donahue et al. (2006), we fit the obtained radial entropy profiles with a three-parameter expression

$$K(R) = \Delta K_0 + K_{100}\left(\frac{R}{100\,h_{71}^{-1}\,{\rm kpc}}\right)^{\alpha}, \qquad (1)$$

where ΔK_0 represents the central gas entropy excess beyond the best-fit power-law model for larger radii, K_{100} is the normalization of the power-law component at $100\,h_{71}^{-1}$ kpc, α is the power-law index, and R is the 3-dimensional radius. All of the best-fit parameters are listed in Table 2. In all systems, the gas entropy profile is well fitted with a power-law model in the outer regions. In nine of the systems, the power-law model can be extrapolated towards the center, resulting in an acceptably good fit. In the other 31 systems, however, there exists a significant central ($R \lesssim 10\,h_{71}^{-1}$ kpc) entropy excess beyond the best-fit power-law model for the outer regions. The obtained central entropy excesses

vary in the range of $0 - 100\,\mathrm{keV\,cm^2}$. This entropy excess is usually mentioned as the central gas entropy plateau, and is suspected to be produced by heat sources like AGNs (e.g., Voit & Donahue 2005; McNamara & Nulsen 2007). Note that in the 2A 0335+096, Abell 85, Abell 496, Abell 3558, Abell 3571, and Abell 4059 clusters, some evidence of minor mergers has been reported in literature (Werner et al. 2006; Durret et al. 2005; Tanaka et al. 2006; Rossetti et al. 2007; Hudaverdi et al. 2005; Choi et al. 2004), which possibly results in mixing of high and low entropy gas (e.g., Ricker & Sarazin 2001; McCarthy et al. 2007). For these clusters, the average slope of the entropy profiles (1.13 ± 0.17) shows no significant systematic bias from those of the sample (1.07 ± 0.28), which indicates that a minor merger likely does not appreciably affect the gas entropy distribution of the sample groups and clusters (Ghizzardi et al. 2010).

3.2 Correlation between Central Gas Entropy Excess and CDG's *K*-band Luminosity

In order to investigate the possible relation between the central gas entropy excess and the AGN heating, we apply the near-infrared *K*-band luminosity L_K of the sample CDG by adopting the apparent *K*-band magnitudes of the CDGs from the Two Micron All Sky Survey (2MASS) archive[1] and converting them into *K*-band luminosities (Table 1). In the calculation, we have corrected Galactic extinction (Schlegel et al. 1998), and applied the correction for redshift (i.e., *k*-correction) as $k(z) = -6\log(1+z)$ (Kochanek et al. 2001).

In Figure 2, we show the central gas entropy excess ΔK_0 versus the *K*-band luminosity L_K for the 40 CDGs in our sample. It can be seen that ΔK_0 apparently increases from 0 to $100\,\mathrm{keV\,cm^2}$ as L_K increases from 1×10^{11} to $3 \times 10^{12}\ L_{K,\odot}$, and ΔK_0 shows a roughly uniform scatter of $\simeq 0.5$ on a logarithmic scale. We find that the correlation coefficient for ΔK_0 and L_K is 0.45, which indicates that the two parameters have a correlation at the 99% confidence level. We have also calculated the Kolmogorov-Smirnov (K-S) statistic of ΔK_0 and L_K against a proper constant model, and find that the correlation has a probability of more than 90% if the null hypothesis is true. Using the bisector of ordinary least-squares regression (Isobe et al. 1990), which is suitable to fit data with large scatters, we fit the $\log \Delta K_0 - \log L_K$ relation with a liner model of

$$\log(\Delta K_0) = A + B\,[\log(L_K/\mathrm{L_{K,\odot}}) - 10.9], \tag{2}$$

and obtain $A = -0.8 \pm 0.3$ and $B = 1.6 \pm 0.4$ (Fig. 2), where the errors are determined by performing the Jackknife simulation that has been repeated 100 times (Feigelson & Babu 1992).

4 DISCUSSION

By analyzing the deprojected gas entropy profiles, we find that there exists a significant central gas entropy excess in 78% of the sample groups and clusters, which can be ascribed to the non-gravitational heating processes. The average central entropy excess ranges from $5.7\,\mathrm{keV\,cm^2}$ to $19.3\,\mathrm{keV\,cm^2}$ from groups to clusters, which corresponds to a gas energy excess of $\simeq 0.1 - 0.2$ and $\simeq 0.3 - 0.5\,\mathrm{keV}$ per gas particle, respectively, when either isodensity or isobaric heating process is assumed (e.g., Lloyd-Davies et al. 2000). Because the observed central entropy excess is correlated to the CDG's *K*-band luminosity, two of the most probable heating sources are AGN activity and supernova explosions. Here, we compare their contributions and determine which one dominates the gas heating process and is thus responsible for the observed central entropy excess. In the calculation that follows, we adopt gravitating mass M_{500} and gas mass fraction $f_{\mathrm{gas},500}$ that are determined at r_{500} (r_{500} is the radius within which the over-density is 500 with respect to the universe's critical density at each system's redshift) following $M_{500} = E(z)^{-1}10^{14.10}(kT_\mathrm{X}/3.0\ \mathrm{keV})^{1.65\pm0.04}\ \mathrm{M_\odot}$ (Sun et al. 2009) and $f_\mathrm{gas} = 0.0708\,(kT_\mathrm{X}/1.0\ \mathrm{keV})^{0.22}$ (Sun et al. 2009; Pratt et al. 2009), respectively, where $E(z) = \sqrt{(1+z)^3\Omega_\mathrm{M} + \Omega_\Lambda}$, and T_X is the mean gas temperature measured in $0.1 - 0.2\,r_{500}$ (Table 2).

[1] See *http://www.ipac.caltech.edu/2mass.*

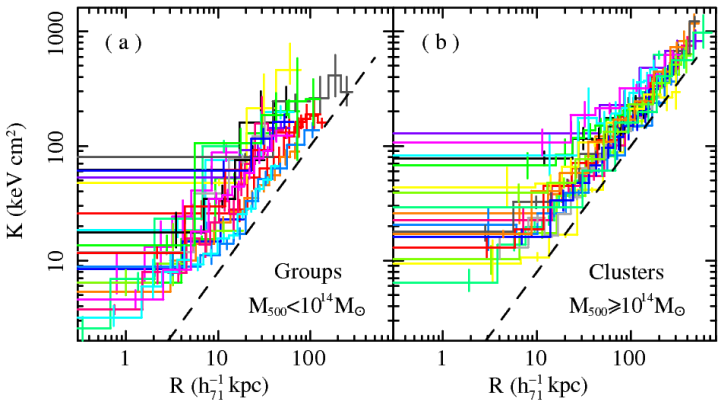

Fig. 1 Deprojected azimuthally-averaged radial distributions of gas entropy $K(R)$ of the galaxy groups ($M_{500} < 10^{14}\,M_{\odot}$; a) and galaxy clusters ($M_{500} \geq 10^{14}\,M_{\odot}$; b) in the sample, along with the theoretical prediction $K \propto R^{1.1}$ with an arbitrary normalization (*dashed lines*), which is ascribed to shock heating that occurred during spherical collapses (Voit & Donahue 2005).

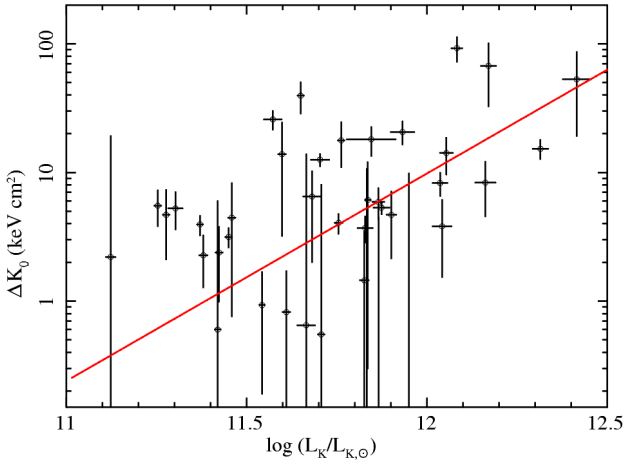

Fig. 2 Central gas entropy excess ΔK_0 vs K-band luminosity L_K for the 40 CDGs of our sample (see also Tables 1 and 2). The solid line shows the best-fit model $\log(\Delta K_0) = -0.8 \pm 0.3 + (1.6 \pm 0.4)[\log(L_K/L_{K,\odot}) - 10.9]$ (Eq. (2) and Sect. 3.2), which is determined by the bisector of ordinary least-squares regression (Isobe et al. 1990).

4.1 AGN Activity

It has been estimated that one powerful AGN outburst can produce a stable entropy excess of $\simeq 10-30\,\mathrm{keV\,cm^2}$ for $\sim 10^8$ yr (Voit & Donahue 2005). In order to obtain the cumulative contribution of AGN feedback that can be approximated by $E^{\rm AGN}_{\rm feedback} \simeq \eta M_{\rm BH}c^2$ (e.g., Croton et al. 2006; Short & Thomas 2009), we calculate the masses of the central black holes hosted in the sample CDGs by applying the relation between the near-infrared K-band luminosity L_K of the host galaxy and the black hole mass $M_{\rm BH}$, i.e., $\log(M_{\rm BH}/M_{\odot}) = 8.21 \pm 0.07 + (1.13 \pm 0.12) \times [\log(L_K/L_{K,\odot}) - 10.9]$,

Table 2 Deprojected Spectral Analysis using an Absorbed APEC+POWERLAW Model

Group/cluster	N_H[a]	ΔK_0[b]	α[c]	K_{100}[d]	T_X[e]	M_{500}[f]	R_{cool}[g]	log (L_X)[h]	$E^{AGN}_{feedback}$[i]	$E^{SN}_{feedback}$[j]	E_{cool}[k]
	(10^{20} cm^{-2})	(keV cm^2)		(keV cm^2)	(keV)	$10^{14}\,M_\odot\,(h_{71}^{-1}$ kpc)		(erg s^{-1})	(keV/gas particle)		
(1)	(2)	(3)	(4)	(5)	(6)	(7)	(8)	(9)	(10)	(11)	(12)
NGC 0383	5.39	$0.55^{+7.47}_{-0.55}$	0.75 ± 0.05	389 ± 47	$2.14^{+1.49}_{-0.60}$	0.72	11	41.06 ± 0.05	2.26	0.0047	0.002±0.0001
NGC 0507	5.24	17.8 ± 6.8	$1.40^{+0.31}_{-0.22}$	179 ± 37	1.55 ± 0.06	0.42	52	$42.40^{+0.09}_{-0.06}$	4.76	0.0123	0.069±0.0002
NGC 0533	3.10	$4.06^{+0.69}_{-0.72}$	1.43 ± 0.04	588 ± 50	$1.72^{+0.65}_{-0.36}$	0.50	25	$42.03^{+0.09}_{-0.12}$	3.85	0.0115	0.024±0.0001
NGC 0720	1.54	$5.52^{+1.74}_{-1.69}$	$0.91^{+0.19}_{-0.11}$	100 ± 44	$0.44^{+0.16}_{-0.21}$	0.05	40	$40.77^{+0.22}_{-0.21}$	13.29	0.0385	0.017±0.0001
NGC 0741	4.43	$6.11^{+5.93}_{-5.81}$	$1.07^{+0.10}_{-0.08}$	420 ± 70	$1.80^{+0.23}_{-0.21}$	0.54	24	$41.62^{+0.06}_{-0.09}$	4.37	0.0139	0.009±0.0001
NGC 1407	5.42	$4.46^{+3.80}_{-3.70}$	$1.36^{+0.12}_{-0.09}$	1440 ± 340	$1.27^{+0.34}_{-0.18}$	0.30	16	$40.81^{+0.15}_{-0.32}$	3.14	0.0102	0.003±0.0001
NGC 2563	4.23	$0.60^{+5.40}_{-0.60}$	1.30 ± 0.05	900 ± 100	$1.69^{+0.18}_{-0.11}$	0.49	17	41.17 ± 0.07	1.66	0.0039	0.003±0.0001
NGC 3402	4.43	$2.39^{+1.38}_{-1.40}$	0.88 ± 0.06	122 ± 11	0.93 ± 0.04	0.18	51	42.49 ± 0.03	5.12	0.0179	0.218±0.0002
NGC 4125	1.84	$4.68^{+2.63}_{-2.57}$	$0.84^{+0.21}_{-0.14}$	83 ± 33	$0.40^{+0.20}_{-0.18}$	0.05	33	$40.55^{+0.23}_{-0.36}$	16.88	0.0750	0.012±0.0001
NGC 4261	1.55	$2.27^{+0.97}_{-0.99}$	1.51 ± 0.06	2480 ± 360	$1.43^{+0.54}_{-0.21}$	0.37	12	$40.78^{+0.07}_{-0.09}$	2.04	0.0072	0.002±0.0001
NGC 4325	2.24	$5.25^{+1.77}_{-1.64}$	1.30 ± 0.09	141 ± 15	$1.07^{+0.03}_{-0.02}$	0.23	58	$42.83^{+0.03}_{-0.04}$	2.89	0.0109	0.370±0.0003
NGC 5044	4.93	$3.95^{+0.65}_{-0.71}$	1.38 ± 0.03	208 ± 8	1.30 ± 0.02	0.32	54	42.60 ± 0.01	2.38	0.0117	0.150±0.0001
NGC 5129	1.76	39.5 ± 10.8	$1.18 \pm^{+0.24}_{-0.18}$	247 ± 55	$0.98^{+0.08}_{-0.05}$	0.20	16	$41.56^{+0.06}_{-0.07}$	8.41	0.0329	0.023±0.0001
NGC 5846	4.26	$3.15^{+0.55}_{-0.54}$	1.33 ± 0.07	431 ± 63	1.01 ± 0.04	0.21	22	$41.50^{+0.17}_{-0.29}$	4.69	0.0131	0.019±0.0001
NGC 6269	4.77	$0.01^{+9.81}_{-0.01}$	0.63 ± 0.08	226 ± 26	$2.53^{+0.28}_{-0.36}$	0.94	31	42.19 ± 0.05	3.13	0.0113	0.017±0.0001
NGC 7619	5.00	$0.93^{+0.75}_{-0.74}$	1.02 ± 0.02	424 ± 21	1.03 ± 0.03	0.21	16	$41.28^{+0.10}_{-0.15}$	5.76	0.0245	0.011±0.0001
HCG 42	4.81	$13.9^{+10.6}_{-10.7}$	$1.47^{+0.42}_{-0.23}$	518 ± 270	$0.93^{+0.10}_{-0.12}$	0.18	21	$41.48^{+0.10}_{-0.09}$	8.06	0.0236	0.021±0.0001
MKW 3S	3.03	$25.9^{+4.2}_{-4.4}$	1.10 ± 0.09	149 ± 9	3.96 ± 0.10	1.95	106	44.02 ± 0.01	0.51	0.0021	0.508±0.0001
MKW 4	1.89	$1.45^{+2.02}_{-1.45}$	0.81 ± 0.04	223 ± 18	$2.00^{+0.07}_{-0.05}$	0.64	47	42.76 ± 0.02	3.50	0.0100	0.099±0.0001
MKW 4S	1.69	$0.01^{+4.45}_{-0.01}$	0.99 ± 0.11	492 ± 137	$1.81^{+0.75}_{-0.48}$	0.54	24	$42.08^{+0.03}_{-0.04}$	4.69	0.0139	0.025±0.0001
UGC 12064	11.8	$2.20^{+17.0}_{-2.20}$	$0.66^{+0.16}_{-0.13}$	244 ± 46	$1.65^{+0.56}_{-0.28}$	0.47	27	$41.62^{+0.06}_{-0.07}$	0.80	0.0032	0.010±0.0001
2A0335+096	20.3(1.78)	3.70 ± 0.85	1.43 ± 0.04	141 ± 5	$4.22^{+0.16}_{-0.13}$	2.18	131	$44.40^{+0.03}_{-0.05}$	0.88	0.0029	1.072±0.0012
Abell 0085	3.42	14.1 ± 4.5	1.09 ± 0.08	174 ± 12	6.32 ± 0.17	4.21	120	$44.44^{+0.03}_{-0.06}$	0.75	0.0014	0.556±0.0008
Abell 0262	5.38	$0.82^{+0.89}_{-0.82}$	1.09 ± 0.03	304 ± 19	2.39 ± 0.05	0.86	47	$42.87^{+0.07}_{-0.05}$	1.43	0.0021	0.091±0.0001
Abell 0478	28.5(1.51)	$3.81^{+2.32}_{-2.27}$	1.06 ± 0.05	150 ± 7	$7.50^{+0.38}_{-0.36}$	5.49	182	$45.17^{+0.04}_{-0.08}$	0.53	0.0013	2.218±0.0039
Abell 0496	4.57	$5.89^{+1.66}_{-1.56}$	1.15 ± 0.05	178 ± 8	5.29 ± 0.09	3.17	109	44.12 ± 0.04	0.63	0.0018	0.369±0.0003
Abell 0780	4.92	$12.6^{+1.3}_{-1.4}$	1.09 ± 0.04	107 ± 4	$3.47^{+0.05}_{-0.06}$	1.57	155	$44.47^{+0.02}_{-0.03}$	0.92	0.0062	1.810±0.0012
Abell 1651	1.81	$53.0^{+33.4}_{-33.8}$	0.80 ± 0.14	234 ± 38	$7.45^{+0.83}_{-0.77}$	5.45	96	44.24 ± 0.02	1.42	0.0006	0.258±0.0001
Abell 1795	1.19	20.7 ± 4.2	1.32 ± 0.10	127 ± 10	6.30 ± 0.20	4.17	148	$44.74^{+0.03}_{-0.06}$	0.55	0.0009	1.104±0.0015
Abell 2029	3.05	15.3 ± 2.6	1.06 ± 0.04	169 ± 6	8.10 ± 0.15	6.28	160	$45.02^{+0.03}_{-0.05}$	0.93	0.0011	1.338±0.0015
Abell 2052	2.73	$5.32^{+0.48}_{-0.58}$	1.48 ± 0.02	210 ± 8	3.20 ± 0.04	1.38	109	$43.95^{+0.04}_{-0.06}$	1.65	0.0022	0.634±0.0009
Abell 2063	2.98	$0.65^{+13.2}_{-0.65}$	0.37 ± 0.12	170 ± 16	3.70 ± 0.15	1.75	90	43.64 ± 0.01	0.75	0.0014	0.239±0.0001
Abell 2199	0.86	$4.68^{+2.42}_{-2.53}$	0.97 ± 0.06	181 ± 9	4.80 ± 0.14	2.70	120	$44.22^{+0.07}_{-0.14}$	0.83	0.0034	0.557±0.0018
Abell 2589	4.14	$0.01^{+10.7}_{-0.01}$	0.45 ± 0.10	208 ± 13	3.64 ± 0.10	1.70	75	43.52 ± 0.01	1.21	0.0021	0.185±0.0001
Abell 3112	2.61	$8.33^{+3.79}_{-3.77}$	1.12 ± 0.13	155 ± 20	$5.56^{+0.30}_{-0.25}$	3.37	138	44.58 ± 0.01	1.23	0.0024	0.984±0.0002
Abell 3558	3.89	$67.4^{+33.6}_{-34.7}$	1.21 ± 0.46	199 ± 41	7.69 ± 0.41	5.83	86	43.92 ± 0.01	0.70	0.0014	0.114±0.0003
Abell 3571	3.71	$92.6^{+20.1}_{-20.0}$	0.94 ± 0.12	193 ± 17	7.17 ± 0.23	5.21	101	$44.26^{+0.01}_{-0.04}$	0.63	0.0024	0.290±0.0003
Abell 4038	1.56	$6.50^{+3.71}_{-4.49}$	0.73 ± 0.10	186 ± 14	3.24 ± 0.11	1.41	78	43.41 ± 0.01	0.98	0.0028	0.180±0.0001
Abell 4059	1.10	$8.28^{+1.64}_{-1.72}$	0.96 ± 0.05	182 ± 6	$4.36^{+0.09}_{-0.08}$	2.29	101	$43.94^{+0.08}_{-0.22}$	1.30	0.0035	0.349±0.0018
MS 0735.6+7421	3.49	$18.1^{+4.5}_{-4.7}$	1.26 ± 0.14	112 ± 17	$5.32^{+0.41}_{-0.32}$	2.94	125	44.56 ± 0.01	0.65	0.0014	1.079±0.0003

[a] Absorptions are fixed to Galactic values (Dickey & Lockman 1990), except for those of 2A 0335+096 and Abell 478, which are left free and shown in brackets (see Sect. 3.1 for details).

[b–d] Central gas entropy excesses, power-law indices, and normalizations of Eq. (1) (Sect. 3.1).

[e] Mean gas temperatures are measured from the spectra extracted within $0.1 - 0.2\,r_{500}$. For each system, the mean gas temperature and r_{500} follow the relation $r_{500} = 391 \times T_X^{0.63}/E(z)$ kpc (Willis et al. 2005).

[f] Total gravitating masses within r_{500} (Sect. 4).

[g] Cooling radii, at which the cooling time equals the universe's age at the system's redshift.

[h] 0.3 – 12.0 keV luminosities are measured within the cooling radius in logarithmic scale.

[i] Cumulative AGN feedback for heating the IGM (Sect. 4 and Fig. 3), which is assumed $E^{AGN}_{feedback} \simeq \eta M_{BH} c^2$ and $\eta = 0.02$.

[j] Supernova feedback for heating the IGM (Sect. 4 and Fig. 3), which includes both type Ia and II supernova contributions.

[k] X-ray Radiative loss since $z = 2$ (Sect. 4 and Fig. 3), which is calculated from the 0.3 – 12 keV luminosity within the cooling radius (R_{cool}).

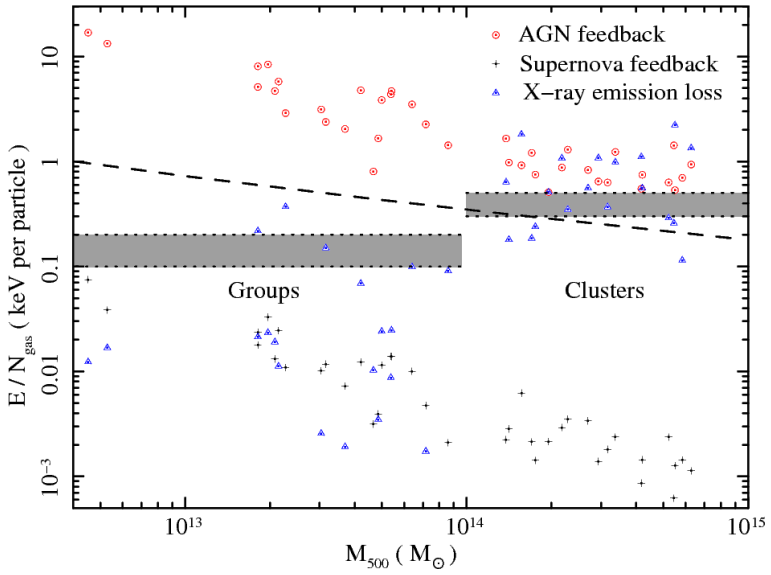

Fig. 3 Estimated energy feedbacks to the IGM by AGNs (*circles*) and supernova explosions (*crosses*), compared to the average gas energy excess of $\simeq 0.1 - 0.2$ and $\simeq 0.3 - 0.5$ keV per particle for galaxy groups and clusters (*grey belts*), respectively; the X-ray radiative loss since $z = 2$ (*triangles*), and the energy required to deviate scaling relations from self-similar predictions (*dashed line*; Bode et al. 2009; see Sect. 4 for details).

which is presented in Marconi & Hunt (2003) and shows similar scatter ranges to the more usually used relation between the stellar velocity dispersion of the galaxy's bulge and $M_{\rm BH}$ (Marconi & Hunt 2003; Batcheldor et al. 2007). We adopt a conversion efficiency of $\eta = 0.02$, because in the study of X-ray cavities in nine elliptical galaxies, Allen et al. (2006) found that about 2% of the accreting energy is converted into the thermal energy of the surrounding gas. By assuming that each gas particle within r_{500} of galaxy groups and clusters has been heated uniformly, we find that the cumulative contribution of AGN feedback varies between $\simeq 0.5 - 17.0$ keV per particle for our sample, which decreases as the gravitating mass M_{500} increases (Table 2 and Fig. 3), and is apparently higher than the average gas energy excess ($\simeq 0.1 - 0.5$ keV per particle).

4.2 Supernova Explosions

Using CDGs' B−band luminosities (L_B; Table 1) and observationally constrained explosion rates of type Ia supernovae (SNe Ia; Dahlen et al. 2004; Cappellaro et al. 2005) and adopting that the supernova explosions heat the surrounding gas with $\sim 10^{50}$ erg per event (e.g., Thornton et al. 1998), we find that the contribution of SNe Ia feedback to the IGM since $z = 3$ (i.e., about $10 - 11$ Gyr ago) is on the order of $\simeq 10^{-4} - 10^{-2}$ keV per particle. On the other hand, we note that, although no type II supernova (SN II) explosions are detected in nearby elliptical galaxies (Cappellaro et al. 1999), the feedback energy of SNe II which exploded at high redshift and in a galaxy's starburst epoch has possibly been deposited and contributed to the gas heating (e.g., Bryan 2000; Wu & Xue 2002). Both field supernova observations in $z = 0.1 - 0.9$ (Dahlen et al. 2004; Cappellaro et al. 2005) and galaxy star formation theories based on initial stellar mass functions (e.g., Kravtsov & Yepes 2000) indicate that the explosion ratio of SNe II to SNe Ia is $\simeq 2 - 3$. This value agrees with the results that were obtained in the studies on IGM metallicity (e.g., Wang et al. 2005; De Grandi & Molendi

2009), which suggested that the explosion ratio of SNe II to SNe Ia is $\simeq 1-6$, the larger scatter of which is probably due to the clusters' different merger histories. By assuming that the feedback energy per SN II event is the same as that of an SN Ia event (e.g., Woosley & Weaver 1986), and that the cumulative explosion ratio of SNe II to SNe Ia is 3, we estimate that the total contribution of supernova feedback to the IGM is $\simeq 0.0006-0.08$ keV per particle, which also decreases as the gravitating mass M_{500} becomes larger (Table 2 and Fig. 3). The estimated supernova contribution is apparently lower than the average gas energy excess ($\simeq 0.1-0.5$ keV per particle), and mostly is about 1–2 orders of magnitude lower than the average gas energy excess. For all the sample groups and clusters, it is about 2–3 orders of magnitude lower than the AGN feedback.

In most cases, the estimated AGN contribution can compensate the radiative loss since $z = 2$ (i.e., about $9-10$ Gyr ago) in galaxy clusters ($\simeq 0.1-2.2$ keV per particle; Table 2 and Fig. 3), which is calculated from the $0.3-12$ keV luminosity within the cooling radius (Table 2). For galaxy groups ($< 10^{14}$ $M_{\odot}$), the AGN feedback energy is about $1-2$ orders of magnitude higher than the X-ray radiative loss ($\simeq 0.002-0.4$ keV per particle; Fig. 3). Moreover, this surplus energy fed by AGNs in galaxy groups is expected to re-distribute the IGM gas, especially in the central regions, and thus break the self-similarity between galaxy groups and clusters. Assuming a uniform baryon (mainly including gas and stellar components) mass fraction for galaxy groups and clusters, the energy required to deviate the scaling relations from the self-similar predictions is $\simeq 0.2-1.0$ keV per particle (Bode et al. 2009), which can be supplied by AGN feedback instead of supernova explosions.

5 SUMMARY

In 31 galaxy groups and clusters, we find that there exists a significant central gas entropy excess, which scales with the K-band luminosity of the CDG via $\Delta K_0 \propto L_K^{1.6\pm0.4}$. By comparing the contributions of AGN activity and supernova explosions, we conclude that AGNs are responsible for the central entropy excesses.

Acknowledgements We thank the *Chandra* team for making data available via the High Energy Astrophysics Science Archive Research Center (HEASARC). This work was supported by the National Natural Science Foundation of China (Grant Nos. 10673008, 10878001 and 10973010), the Ministry of Science and Technology of China (Grant No. 2009CB824900/2009CB24904), and the Ministry of Education of China (the NCET Program).

References

Allen, S. W., Dunn, R. J. H., Fabian, A. C., Taylor, G. B., & Reynolds, C. S. 2006, MNRAS, 372, 21
Batcheldor, D., Marconi, A., Merritt, D., & Axon, D. J. 2007, ApJ, 663, L85
Birzan, L., Rafferty, D. A., McNamara, B. R., Nulsen, P. E. J., & Wise, M. W. 2009, arXiv: 0909.0397
Bode, P., Ostriker, J. P., & Vikhlinin, A. 2009, ApJ, 700, 989
Bondi, H. 1952, MNRAS, 112, 195
Bryan, G. L. 2000, ApJ, 544, L1
Cappellaro, E., Evans, R., & Turatto, M. 1999, A&A, 351, 459
Cappellaro, E., et al. 2005, A&A, 430, 83
Cavagnolo, K. W., Donahue, M., Voit, G. M., & Sun, M. 2008, ApJ, 683, L107
Choi, Y.-Y., Reynolds, C. S., Heinz, S., Rosenberg, J. L., Perlman, E. S., & Yang, J. 2004, ApJ, 606, 185
Croton, D., J. et al. 2006, MNRAS, 365, 11
Dahlen, T., et al. 2004, ApJ, 613, 189
De Grandi, S., & Molendi, S. 2009, A&A, 508, 565
Dickey, J. M., & Lockman, F. J. 1990, ARA&A, 28, 215
Donahue, M., Horner, D. J., Cavagnolo, K. W., & Voit, G. M. 2006, ApJ, 643, 730

Durret, F., Lima Neto, G. B., & Forman, W. 2005, A&A, 432, 809
Feigelson, E. D., & Babu, Gutti J. 1992, ApJ, 397, 55
Ghizzardi, S., Rossetti, M., & Molendi, S. 2010, arXiv:1003.1051
Hudaverdi, M., Yamashita, K., & Furuzawa, A. 2005, Advances in Space Research, 36, 643
Ikebe, Y., Reiprich, T. H., Böhringer, H., Tanaka, Y., & Kitayama, T. 2002, A&A, 383, 773
Isobe, T., Feigelson, E. D., Akritas, M. G., & Babu, G. J. 1990, ApJ, 364, 104
Jetha, N. N., Ponman, T. J., Hardcastle, M. J., & Croston, J. H. 2007, MNRAS, 376, 193
Kaiser, N. 1986, MNRAS, 222, 323
Kochanek, C. S., Pahre, M. A., Falco, E. E., et al. 2001, ApJ, 560, 566
Kravtsov, A. V., & Yepes, G. 2000, MNRAS, 318, 227
Lloyd-Davies, E. J., Ponman, T. J., & Cannon, D. B. 2000, MNRAS, 315, 689
Marconi, A., & Hunt, L. K. 2003, ApJ, 589, L21
Mathur, S., Stoll, R., Krongold, Y., Nicastro, F., Brickhouse, N., & Elvis, M. 2009, arXiv: 0910.3691
Mazzotta, P., Edge, A. C., & Markevitch, M. 2003, ApJ, 596, 190
McCarthy, I. G., Bower, R. G., Balogh, M. L., et al. 2007, MNRAS, 376, 497
McNamara, B. R., & Nulsen, P. E. J. 2007, ARA&A, 45, 117
Mulchaey, J. S., Davis, D. S., Mushotzky, R. F., & Burstein, D. 2003, ApJS, 145, 39
Navarro, J. F., Frenk, C. S., & White, S. D. M. 1995, MNRAS, 275, 720
Osmond, J. P. F., & Ponman, T. J. 2004, MNRAS, 350, 1511
Paturel, G., Petit, C., Prugniel, Ph., et al. 2003, A&A, 412, 45
Ponman, T. J., Sanderson, A. J. R., & Finoguenov, A. 2003, MNRAS, 343, 331
Pratt, G. W., Croston, J. H., Arnaud, M., & Böhringer, H. 2009, A&A, 498, 361
Rafferty, D. A., McNamara, B. R., Nulsen, P. E. J., & Wise, M. W. 2006, ApJ, 652, 216
Rafferty, D. A., McNamara, B. R., & Nulsen, P. E. J. 2008, ApJ, 687, 899
Ricker, P. M., & Sarazin, C. L. 2001, ApJ, 561, 621
Rossetti, M., Ghizzardi, S., Molendi, S., & Finoguenov, A. 2007, A&A, 463, 839
Sanderson, A. J. R., Finoguenov, A., & Mohr, J. J. 2005, ApJ, 630, 191
Schlegel, D. J., Finkbeiner, D. P., & Davis, M. 1998, ApJ, 500, 525
Short, C. J., & Thomas, P. A. 2009, ApJ, 704, 915
Sun, M., Voit, G. M., Donahue, M., Jones, C., Forman, W., & Vikhlinin, A. 2009, ApJ, 693, 1142
Tanaka, T., Kunieda, H., Hudaverdi, M., Furuzawa, A., & Tawara, Y. 2006, PASJ, 58, 703
Thornton, K., Gaudlitz, M., Janka, H.-Th., & Steinmetz, M. 1998, ApJ, 500, 95
Voit, G. M., & Donahue, M. 2005, ApJ, 634, 955
Wang, Y., Xu, H., Zhang, Z., Xu, Y., Wu, X.-P., Xue, S,-J., & Li, Z. 2005, ApJ, 631, 197
Werner, N., de Plaa, J., Kaastra, J. S., et al. 2006, A&A, 449, 475
White, R. L., Helfand, D. J., Becker, R. H., Glikman, E., & de Vries, W. 2007, ApJ, 654, 99
Willis, J. P., et al. 2005, MNRAS, 363, 675
Woosley, S. E., & Weaver, T. A. 1986, ARA&A, 24, 205
Wu, X.-P., & Xue, Y.-J. 2002, ApJ, 569, 112